Journal of
Synchrotron Radiation

ISSN 0909-0495

Received 25 August 2008
Accepted 11 January 2009

A curved image-plate detector system for high-resolution synchrotron X-ray diffraction

P. Sarin,[a] R. P. Haggerty,[a] W. Yoon,[a] M. Knapp,[b] A. Berghaeuser,[c] P. Zschack,[d] E. Karapetrova,[d] N. Yang[d] and W. M. Kriven[a]*

[a]Department of Materials Science and Engineering, University of Illinois at Urbana-Champaign, IL 61801, USA, [b]Institute for Materials Science, Darmstadt University of Technology, Darmstadt D-64287, Germany, [c]Institute for Mineralogy and Petrography, University of Hamburg, Hamburg D-20146, Germany, and [d]Advanced Photon Source, Argonne National Laboratory, Argonne, IL 60439, USA. E-mail: kriven@illinois.edu

The developed curved image plate (CIP) is a one-dimensional detector which simultaneously records high-resolution X-ray diffraction (XRD) patterns over a 38.7° 2θ range. In addition, an on-site reader enables rapid extraction, transfer and storage of X-ray intensity information in $\leq$30 s, and further qualifies this detector to study kinetic processes in materials science. The CIP detector can detect and store X-ray intensity information linearly proportional to the incident photon flux over a dynamical range of about five orders of magnitude. The linearity and uniformity of the CIP detector response is not compromised in the unsaturated regions of the image plate, regardless of saturation in another region. The speed of XRD data acquisition together with excellent resolution afforded by the CIP detector is unique and opens up wide possibilities in materials research accessible through X-ray diffraction. This article presents details of the basic features, operation and performance of the CIP detector along with some examples of applications, including high-temperature XRD.

Keywords: X-ray detectors; image-plate detector; powder diffraction; high-resolution diffraction; *in situ* diffraction.

1. Background

X-ray powder diffraction is a valuable cornerstone in materials characterization. Over the last two decades this technique has been increasingly used to solve crystal structures using the Rietveld method, a development which has greatly enhanced the power of the powder diffraction method (Rietveld, 1969). Advancements made in instrumentation and computer technology have also contributed to the growth in popularity of the powder diffraction method. Instrumental developments have been focused on improving the quality of diffraction data as well as on decreasing the time required for measurements. Furthermore, the advent of synchrotron X-ray sources has propelled the need to develop X-ray detectors to conduct dynamic studies in real time (Hall & Lewis, 1994). Amongst the various detector systems which have been considered in the past are (i) multi-detector systems (Fitch, 2004; Lee *et al.*, 2008) and (ii) position-sensitive detectors (PSDs), which include linear sensitive proportional counters (Evain *et al.*, 1993; Shishiguchi *et al.*, 1986; Wölfel, 1983), charge coupled devices (*i.e.* CCDs) and image-plate (IP) systems (Amemiya, 1995; Norby, 1997; Ståhl, 2000). Although the multi-detector set-up, when used along with the analyzer crystals, provides for unparalleled resolution in X-ray diffraction data, it could still require some time to collect diffraction patterns suitable for structure solution (Fitch, 2004; Lee *et al.*, 2008). Regardless of the angular coverage of each analyzer detector in the multi-detector set-up, the diffraction data are collected by scanning procedures and have associated angular time dependence. PSDs belong to the category of X-ray detectors which utilize different phenomena of X-ray interaction with matter to record the positions of the arrival of X-ray photons. These detectors offer the advantage of simultaneous acquisition of diffraction data over a large 2θ range. More recently, research has focused on the use of photon-counting silicon microstrip detector arrays (Fauth *et al.*, 2000). When used in Guinier geometry, it is possible to achieve resolution approaching that of an analyzer crystal set-up (Siddons *et al.*, 2007). Although several detector systems have been developed to date, and some are even commercially available, no dominant PSD detector design has been established. Research is ongoing to develop PSD systems which can offer higher resolution, faster data acquisition rates and simple calibration without compromising the signal-to-noise (S/N) ratios.

Arndt has discussed several characteristics to assess the quality of a PSD (Arndt, 1986). Among these, cost is the most prohibitive factor. Construction of a fast PSD system to cover a wide 2θ range with adequate spatial resolution can be

expensive, particularly in systems which use linear sensitive proportional counters or CCDs. IP detectors which use a phosphor film tend to be less expensive and have been developed both as flat plates (Gualtieri *et al.*, 1996; Rizzo *et al.*, 1995; Thoms *et al.*, 1996) and as cylindrical curved detectors (Fujiwara *et al.*, 2000; Garrett *et al.*, 1995; Kellermann *et al.*, 2001; Nishibori *et al.*, 2001*a*,*b*). However, one problem with the IP detectors has been the delay in data acquisition, either owing to the size of the area detector or to the requirement of an external scanner, which can also compromise reproducibility.

A new one-dimensional curved image plate (CIP) detector has been developed to rapidly collect powder diffraction patterns with excellent angular resolution and good dynamic range performance. This detector is based on the OBI (Ortsfestauslesbarer Bildplattendetektor) detector previously developed at Hamburger Synchrotronstrahlungslabor (HASYLAB) at the Deutsches Elekronen-Synchrotron (DESY), Hamburg, Germany (Knapp, Baehtz *et al.*, 2004; Knapp, Joco *et al.*, 2004). The restriction of the detector to one dimension (as opposed to a two-dimensional IP) reduces the complexity of the mechanics and the time for the readout of the IP. The CIP detector is a significant improvement over all other position-sensitive detectors for rapid collection of high-resolution data. The detector has been designed for operation in conjunction with a quadrupole lamp furnace (QLF) to conduct *in situ* high-temperature X-ray diffraction (HTXRD) studies on polycrystalline (or powder) specimens, in real time, up to 2273 K in air (Sarin, Jurkschat *et al.*, 2006). This article presents details on the basic features, operation and performance of the CIP detector along with some examples of applications.

2. Basic components and design

The CIP detector is a curved one-dimensional detector which simultaneously records the entire X-ray diffraction pattern over a 38.7° 2θ range on a photostimulable curved image plate. Fig. 1 shows a side view of the CIP detector mounted for use at the 33BM-C beamline at the APS at ANL, Argonne, IL, USA. The salient parameters and components of the CIP detector are listed in Table 1. The details of the working and construction of the CIP detector are analogous to the OBI detector at HASYLAB, and have been reported elsewhere (Knapp, Baehtz *et al.*, 2004; Knapp, Joco *et al.*, 2004). The detector is constructed as a section of a circle of radius 1045 mm, with the polycrystalline sample at its center. The photostimulable phosphor IP (Fujifilm BAS-IP SR 2040) is glued onto a cylindrically curved aluminium plate which is encased in a light-tight housing made of aluminium and lead. A 15 mm-wide slit in front of the IP allows for exposure to X-radiation over the full angular range of the detector. The slit is also covered with a black carbon impregnated Kapton foil to protect the IP from exposure to ambient visible light.

Upon exposure to X-rays, a latent image is generated in the form of locally trapped electron–hole pairs (von Seggern, 1999). Only a fraction of incident X-ray energy is stored, which can later be stimulated by visible light to induce photostimulated luminescence (PSL). The intensity of the light emitted as a result of PSL, which has a wavelength of 390 nm, is proportional to the absorbed X-ray intensity (Sonoda *et al.*, 1983). In the CIP detector the absorbed X-ray intensity

Table 1
CIP detector components and specifications.

Phosphor image plate	
Type	Fujifilm BAS-IP SR 2040
2θ coverage	∼40°
Sample-to-plate distance	∼1045 mm
Arc length of phosphor plate	∼700 mm
Scanner head, motor and eraser	
Scanning laser diode, dimensions on IP	2.4 mm × 0.025 mm (W × H)
Scanning laser diode, power output	3 mW
Scanning laser diode, wavelength	635 nm (red)
Photostimulated luminescence wavelength	390 nm
Integrating optical sphere, diameter	34 mm
Blue glass filter	Schott-glass BG3
Photomultiplier tube, type	Hamamatsu H5784
Motor servo amplifier, type	Danaher-Motion Servostar 406M
Motor optical encoder, type	Renishaw RGH22
Eraser halogen lamp bulb, type	OSRAM Decostar 35 (30 W)
CIP detector overall physical parameters	
Total detector weight	∼110 kg
Total length (in beam direction)	∼1000 mm
Total height	∼1550 mm
Total width	∼510 mm
Plate aluminium housing (inner and outer diameter)	850 mm and 1070 mm
Supporting aluminium construct (H × L × W)	810 mm × 950 mm × 650 mm

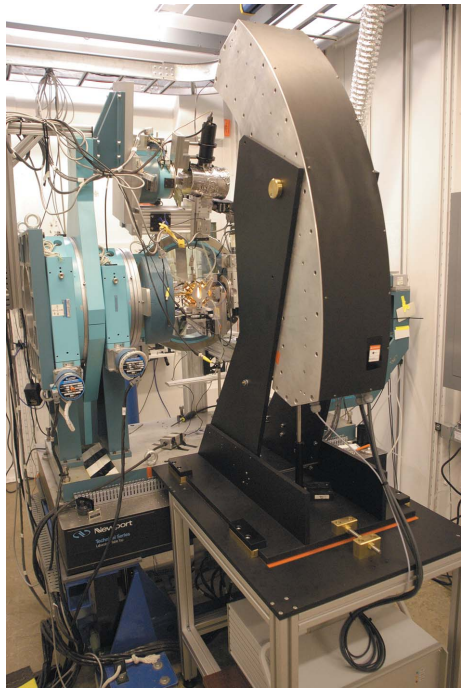

Figure 1
The curved image plate (CIP) detector at the 33BM-C beamline at APS. Also shown in the photograph is the quadrupole lamp furnace mounted on the Huber diffractometer, and, together with the CIP detector, this equipment was used for HTXRD investigations on polycrystalline or powder samples in air, up to 2273 K.

information is extracted using a scanner consisting of an adjustable line focus red laser diode [2.4 mm (W) × 0.025 mm (H)] for stimulation, and a photomultiplier tube (PMT; Hamamatsu H5784) to record the emitted light. Both the scanning laser diode as well as the PMT are shielded in a specially designed scanner head. The scanner head is fixed onto a mobile carriage guided by a curved rail and is driven by a linear motor. Its position can be determined with an accuracy of better than 1 μm. The output voltage from the PMT is converted by an analogue/digital converter in real time, and 40900 data points, in the form of observed intensity *versus* pixel number, are transferred *via* TCP/IP to the data collection computer. The remaining image on the IP is then erased by a halogen lamp, which is placed next to the scanner head, to prepare the detector for the next exposure.

The CIP detector was designed for use at the 33BM-C beamline at the APS at ANL, and has high intrinsic resolution. The data acquisition time is short owing to significant X-ray intensities at the APS. The CIP detector system permits simultaneous measurement of the powder diffraction spectrum over a large range of scattering angles. Taking into account the angular coverage of the CIP and the total number of data points, the detector has an angular pitch of $\sim$0.00095°. The choice of a smaller angular range for the CIP detector was mainly dictated by the accessible 2θ range of the QLF, as it is primarily intended for X-ray diffraction (XRD) studies on polycrystalline samples at high temperatures (Sarin, Haggerty *et al.*, 2006; Sarin, Jurkschat *et al.*, 2006). The larger sample-to-IP distance (1045 mm) in the CIP detector set-up enables collection of XRD patterns with higher resolution. It also permits the use of a crystal analyzer set-up without any repositioning of the CIP detector, which is essential for the determination of 2θ values for each pixel on the CIP, as explained in the next section.

3. Set-up and operation

3.1. Detector alignment and calibration

The first task in the configuration of the CIP detector is the alignment, followed by calibration, which involves the assignment of 2θ values to each pixel on the IP. The alignment process involves positioning the CIP such that each point on the image plate is equidistant, approximately 1045 mm, from the sample mounted on the Huber diffractometer. The alignment is performed upon first use of the detector, and the detector position is fixed for subsequent experimental runs. The CIP detector is mounted on a stand attached to a table, and has four degrees of freedom for manual positioning of the detector. While the table allows for linear translation, both perpendicular to and along the incident X-ray beam direction, a rotational adjustment on the stand about an axis parallel to the sample axis enables finer angular positioning of the CIP.

The pixels on the CIP detector were assigned 2θ values with an accuracy of 0.0006° using the diffraction pattern from LaB_6 powder, the standard reference material (SRM 660a) from the National Institute of Standards and Technology (NIST, Gaithersburg, MD, USA). The powder standard was mounted in a 0.2 mm glass capillary (Glas, W. Muller, Schönwalde, Germany) and rotated at 60 r.p.m. An incident slit of 0.2 mm (H) × 3 mm (W) and a wavelength of 0.5508 Å were used for these measurements. The output of the CIP detector is in the form of absorbed X-ray intensity *versus* pixel number. In order to assign a 2θ value to each pixel on the IP, the LaB_6 peak positions, measured as pixel numbers by the CIP detector, were compared with 2θ values for the corresponding peaks measured using a scintillation counter with a Si (111) analyzer crystal in the diffracted beam path. A polynomial of second order was calculated by least-squares routines to transform the pixel values on the CIP to 2θ values. Fig. 2 shows the deviation in the 2θ position determined using the CIP detector from the true 2θ position which was measured using the crystal analyzer. The random distribution of residuals around true 2θ values (*i.e.* when Residual = 0 in Fig. 2) justifies the choice of the second-order polynomial function. Since the IP detector is curved, an ideal alignment should result in a linear function to transform pixels to 2θ values. As shown in Fig. 2 (see inset), the second-order transformation polynomial for 2θ assignment was fairly linear, considering the small value of the B_2 coefficient. After satisfactory alignment and 2θ assignment of the pixels the CIP detector produces high-quality results in XRD experiments.

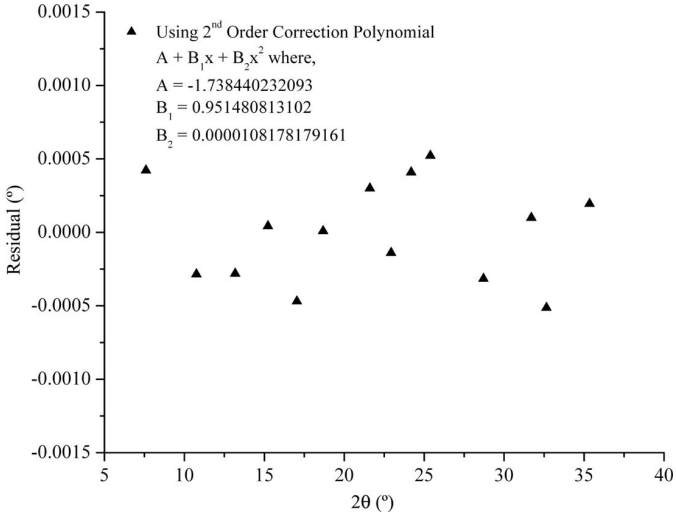

Figure 2
Calibration of pixels on the CIP detector using SRM 660a reference (LaB_6 powder) standard. The error in the assignment of 2θ values to each pixel was negligible (<0.0005°). (Note that in the second-order correction polynomial, x = pixels/1000.)

3.2. Improvement of S/N and/or time resolution

The CIP detector operation can be optimized to yield improved S/N ratios and/or time resolution in XRD experiments. A number of factors can determine the time resolution of an XRD experiment, and include (i) detector characteristics such as rate of recording of incident X-ray photons and retrieval of intensity information, (ii) exposure time, and (iii) automation of the experiment. The CIP detector, which is an integrating detector based on IP technology, is not constrained

by instantaneous count-rate limitations. Since the response time of the PSL phenomena is <1 μs (Amemiya & Miyahara, 1988), the rate-determining step for intensity information retrieval is the speed with which the scanner head can be moved across the CIP. The extraction of X-ray intensity and subsequent erasure of any residual information on the CIP can take approximately 30 s. Exposure time is mainly a sample-dependent variable and various factors such as absorption by the sample, extent of crystallinity of the sample, as well as the beam intensity can determine the duration of each scan. Automation of the XRD experiments is also important to achieve good time resolution. All relevant aspects of a synchrotron XRD experiment which include the CIP detector operation, opening and closing of the 33BM-C beamline shutters for different exposure times or incident photon count, and other experimental controls (*e.g.* temperature control for HTXRD experiments) can be automated. In addition to the beamline components, a separate pneumatic shutter was designed and integrated with the CIP detector operation for precise control of time of exposure of the sample to the X-ray beam during an experimental measurement.

For XRD experiments where time resolution is not very critical, the S/N factor could be enhanced by summation or averaging of several scans acquired from multiple exposures. The time required for an XRD experiment could also be reduced by operational procedures without significantly compromising the S/N ratio of the diffraction pattern. This was possible by multiple readings of the X-ray intensity information stored in the IP from a single exposure. During the intensity readout process the laser induces only a fraction of the possible PSL at a given location on the IP. As a result, the read process could be repeated a second time before the IP was erased. In order to compare the effect of multiple readings of the same exposure of the CIP, XRD patterns were acquired using the LaB_6 powder sample for different incident intensities, and each exposure was read twice. Fig. 3(*a*) compares the intensities from the first reading (r1) with the sum of the first and second readings (r1 and r2, respectively) for the 111 and the 100 peaks for LaB_6. The linear scaling of the peak intensities with increasing incident intensities for both the cases, *i.e.* r1 and r1+r2, confirmed that the peak intensities measured during the second reading are proportional to the first reading. Furthermore, it is also arguable that combining r1 and r2 may also improve the achievable S/N ratio of the XRD pattern. Since the X-ray information storage, stimulation and detection in an IP detector are probabilistic processes, the second reading can improve the counting statistics. The stochastic behavior of the IP counting will lead into saturation of S/N, whereas the effect of other contributions from the system/electronics can be improved by multiple readings, mainly influencing the background of the pattern. The resolution of the XRD pattern was also not altered between r1 and r2, and is shown in Fig. 3(*b*). Similarity in the values of the Caglioti's parameters *U*, *V* and *W* (Caglioti *et al.*, 1958) for the cases of r1, r2 and r1+r2, presented as in inset table in Fig. 3(*b*), confirms this result quantitatively. However, the benefit of multiple readings of the same scan is limited and

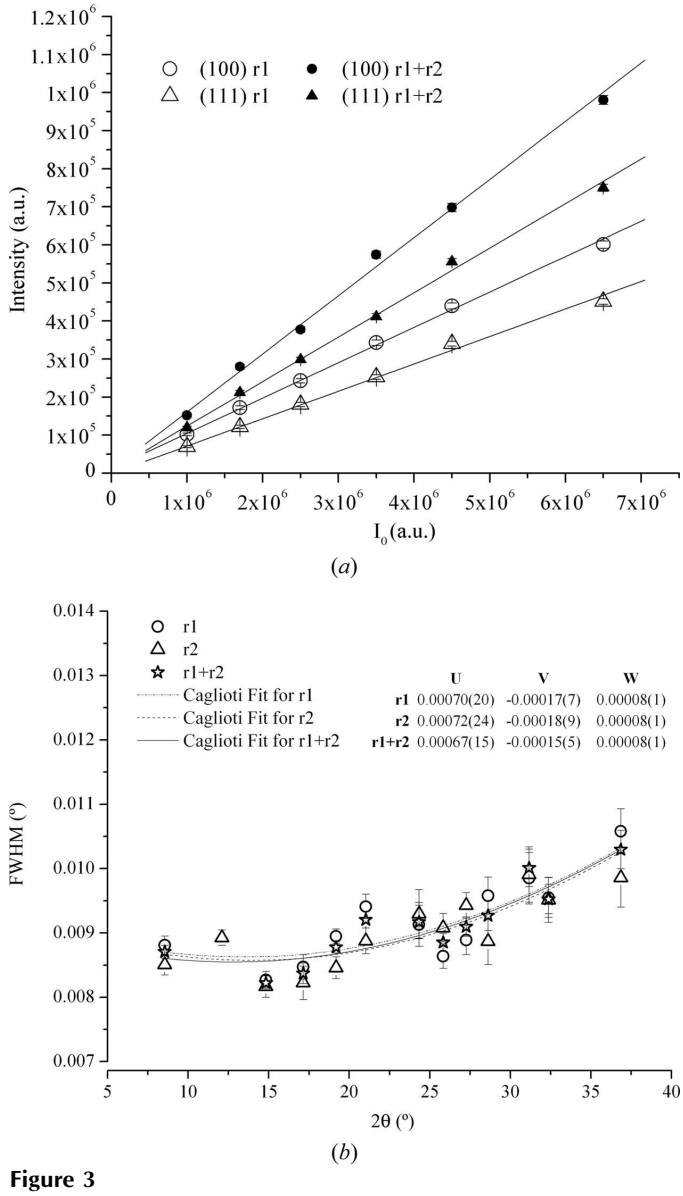

Figure 3
Addition of two readings from a single exposure of the CIP detector does not compromise (*a*) the linearity of the detector response or (*b*) the resolution of the detector.

cannot be derived infinitely. During each reading, partial information is erased from the IP and the measured intensities decreased in each subsequent reading. Nonetheless, multiple readings of the same exposure decreased the time required to collect XRD patterns with reasonable S/N ratio when compared with data acquisition using multiple exposures. However, this mode of operation does increase the time interval between two consecutive exposures.

4. Performance characteristics and applications

The CIP detector inherits all the advantages commonly associated with IP detectors, such as high count-rate capability, a wide dynamic range, uniformity of response *etc.* (Miyahara *et al.*, 1986). In addition, this detector configuration also overcomes the usual limitations encountered with the IP detectors

such as the requirement for an external scanner, or a small accessible angular range, as well as low spatial resolution. In this study, extensive care was taken to identify the advantages and any limitations of the CIP detector to conduct powder XRD investigations. Some of the results reported in this article are confirmation of already accepted characteristics of IP detector systems. Their inclusion in this article was considered necessary for quantitative representation of the performance of the CIP detector when used for powder XRD studies at synchrotron sources. Other studies are presented to highlight the significant advantages of the CIP detector to address challenging problems encountered in materials science using powder XRD.

All experiments were performed at the bending-magnet beamline at 33BM-C at APS, ANL, Argonne, IL, USA. Standard reference materials 660a (LaB_6) and 674a (α-Al_2O_3, TiO_2, ZnO and Cr_2O_3) from NIST (Gaithersburg, MD) were used to evaluate the detector performance. Powder samples of these materials were mounted in glass capillaries, rotated at 60 r.p.m., and XRD patterns were acquired in transmission geometry. In the following sections the CIP detector performance and selected applications are discussed.

4.1. Instrumental resolution

The most important benchmark for detector performance in powder XRD experiments is instrumental resolution. Precise determination of peak positions and the ability to resolve two peaks in very close proximity rely on high spatial resolution. The resolution of a diffractometer, which is also the intrinsic instrumental broadening owing to wavelength dispersion, aberrations *etc.*, can be ascertained using a reference material that does not yield extra broadening because of crystallite size and/or strain effects. SRM 660a (LaB_6) from NIST is specially prepared to fulfil these criteria and was used for this analysis. Instrumental resolution was determined by measurement of the full width at half-maximum (FWHM) of the Bragg peaks in the XRD pattern of the standard. Fig. 4 compares the FWHM of the Bragg reflections from the XRD patterns collected using the CIP detector and the Si (111) analyzer crystal for SRM 660a samples mounted in capillaries of different sizes. All the patterns were acquired using incident X-rays of wavelength 0.7006 Å and an incident slit size of 0.5 mm (H) × 3 mm (W).

The reflection half-width of the LaB_6 (110) peak measured for a 0.1 mm capillary sample using the CIP detector was 0.007°. In comparison, the FWHM of the XRD pattern acquired using the Si (111) analyzer crystal was 0.004°. The instrumental resolution achievable using the CIP detector is much higher than any point detector or IP detector system. It further translates into an accuracy of at least 0.001° in 2θ for peak position determination or approximately 0.0001 Å in lattice spacing measurements. Increase in sample size (*i.e.* capillary size) resulted in deterioration of resolution. Assuming a parallel incident X-ray beam, a simplifying assumption for the 33BM-C bending-magnet beamline, the main contribution to the instrumental resolution function in this set-up is the projection of the capillary onto the IP. Therefore, reflection half-widths and peak shapes are influenced by the capillary diameter and the distance between capillary and IP. Considering the sample-to-IP distance (1045 mm), the size of the focal spot of the laser beam from the scanner (0.025 mm), the grain size of the IP materials and the typical size of a sample (0.3 mm), a FWHM of reflections below 0.02° is achievable with the CIP detector. The sample size had no effect on the FWHM of XRD patterns acquired using a Si (111) analyzer crystal (not shown), which functions as an angular slit rather than a linear slit with finite dimensions. The curve of the FWHM *versus* 2θ is expected to follow Caglioti's empirical equation, $\mathrm{FWHM}^2 = U\tan^2\theta + V\tan\theta + W$ (Caglioti *et al.*, 1958). The calculated values for the U, V and W parameters for different capillary size samples are presented in Table 2. The peak shapes for sample capillary sizes of 0.3 mm and 0.5 mm were 'super-Gaussian' in nature, and could not be fitted with a pseudo-Voigt function. The FWHM values for the 0.3 mm and 0.5 mm capillary samples included in Fig. 4 were approximated using a Gaussian function, and did not yield reasonable U, V and W parameters when fitted with the Caglioti function.

Table 2
Caglioti formula parameters U, V and W determined for different capillary samples using LaB_6 standard.

	U	V	W
Analyzer	0.00036 (3)	−0.00007 (1)	0.00002 (0)
0.1 mm capillary	0.00039 (9)	−0.00001 (3)	0.00004 (0)
0.2 mm capillary	0.00057 (11)	−0.00013 (4)	0.00009 (0)

A crystal analyzer inserted between the sample and a conventional detector remains the highest resolution detector for X-ray powder diffraction (Hastings *et al.*, 1984), but the advantages of this technique come at the cost of greatly reduced intensity and exceedingly long data acquisition times. The CIP detector successfully transcends these limitations and

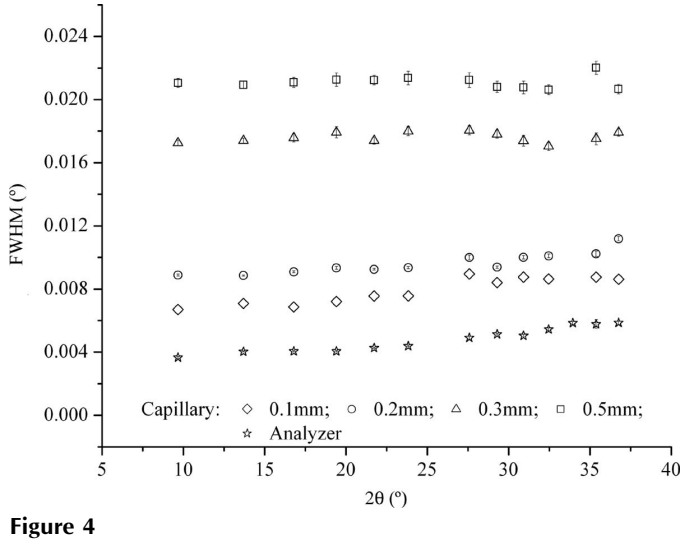

Figure 4
Comparison of FWHM measured using the LaB_6 standard for different capillary sizes, at the same incident wavelength.

combines high speeds in data acquisition over a wide dynamic range with excellent resolution.

4.2. Linearity of response

Linearity and uniformity of response are two important characteristics of a position-sensitive X-ray detector. Linearity is the ability of an X-ray detector to respond proportionally to the incident photon flux. On the other hand, the uniformity of response of a PSD is its ability to produce an identical response, with minimal variations at each pixel, for the same exposure to an incident X-ray photon flux. This is an important consideration for quantitative analysis and crystal structure refinement. The response of the PSL phenomena for an IP was reported to be linear over the range 8×10^1 to 4×10^4 photons $(100\ \mu m)^{-2}$, with an error rate of less than 5% (Amemiya, 1995). In general, the IP detector systems are expected to show a linear response over their dynamic range (1 to $\sim 10^5$) and to yield reproducible results over long periods of repeated use (Amemiya & Miyahara, 1988; Thoms *et al.*, 1998).

The performance of the CIP detector was found to be linear over a wide range of incident photon flux (I_0 = 0.5, 1.5, 1.7, 2.5, 4.5 and 6.5×10^6 a.u.) at constant energy (~20.0 keV) with no loss in resolution. For this purpose a series of XRD patterns were acquired using the LaB_6 standard (SRM 660a) powder mounted in a 0.1 mm glass capillary, for a range of incident X-ray photon flux. An ion chamber in the incident beam path was used to monitor the incident photon count (proportionally). All the XRD patterns were collected using X-rays with λ = 0.6194 Å. Peak intensities were determined by fitting each peak individually with a pseudo-Voigt function [ηL + (1 − η)G; where η is the mixing parameter for Gaussian (G) and Lorentzian (L) profiles] using *CMPR* (Toby, 2005). Fig. 5(*a*) shows the change in intensity with increasing incident photon flux for several peaks of the LaB_6 standard. A plot of FWHM *versus* 2θ for all the acquired patterns is shown in Fig. 5(*b*), and confirms that the instrumental resolution was invariant with incident intensity flux. With increasing exposure the 110 peak was saturated for $I_0 = 4.5 \times 10^6$ and 6.5×10^6, and showed a plateau at the apex. Therefore, the peak intensities and FWHM for these peaks are not included in Figs. 5(*a*) and 5(*b*). The saturation limit for intensity counts for the CIP detector is set at 65536 (*i.e.* 2^{16}), and intensity counts larger than this limit appear as a plateau. It is important to note that despite the saturation in some of the peaks the linearity and peak shape of the unsaturated peaks were not affected. Overall, the proportional increase in the intensity of each peak with incident photon flux, observed with the CIP detector, is consistent with the expected linearity of response of an IP detector system.

Some measure of uniformity in response of the CIP may be gauged from the invariance in relative intensities of all the 14 peaks for LaB_6, within a reasonable margin of error for IP systems (~5 to 6%). These peaks were distributed throughout the 2θ range which extended from 0 to 37°. However, the uniformity of an IP detector is best ascertained by examining

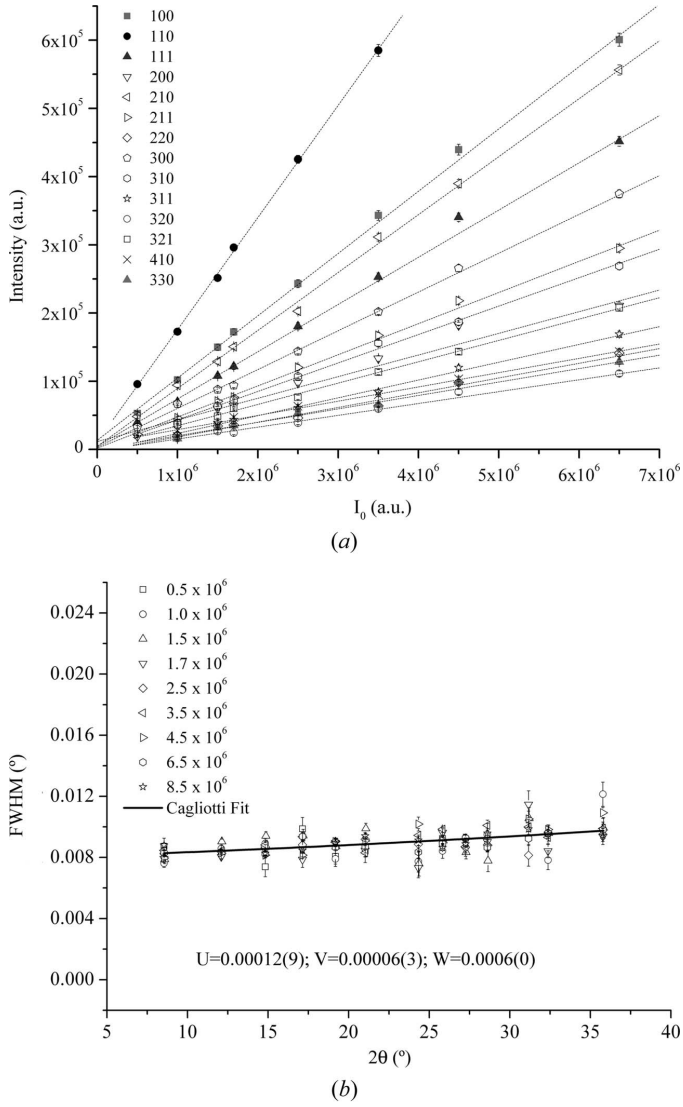

Figure 5
The performance of the CIP detector over a wide range of incident I_0 at constant energy is (*a*) linear and (*b*) without any loss in resolution.

the response of each pixel under uniform illumination/exposure. This is particularly difficult in the case of the CIP detector because of the extent of angular coverage. An alternative approach could involve exposing each pixel on the detector to the same flux by moving the detector across the X-ray beam with a finite slit placed in front of it. Unfortunately the size and weight of the detector are not suitable for such an experiment.

4.3. Effect of incident X-ray energy

The CIP detector performance was also evaluated as a function of incident X-ray energy in terms of spatial resolution. As shown in Fig. 6, the instrumental resolution of the CIP detector was invariant for incident X-radiation with energies ranging from 14.0 to 22.5 keV. These experiments were conducted using the SRM 660a LaB_6 powder mounted in 0.2 mm glass capillaries, and rotated at 60 r.p.m. The sample was exposed for different durations to achieve an adequate

S/N ratio in the observed diffraction profile. Each of the Bragg peaks was fitted with a pseudo-Voigt function using *CMPR*. The mixing parameter η remained fairly uniform throughout the 2θ range for all the energies. The instrumental resolution was also compared with the FWHM measured using a Si (111) analyzer crystal. The slightly lower resolution observed in the 14.0 keV data set was observed for both the CIP detector and the Si crystal analyzer. This might be attributed to the focusing condition of the incident beam.

Table 3
Experimentally measured lattice constants for several X-ray powder diffraction standard reference materials.

		a (Å)	σ	c (Å)	σ	R_p
α-Al_2O_3	NIST	4.759397	0.000080	12.992370	0.000220	
	Present study	4.759334	0.000004	12.992232	0.000019	3.66
ZnO	NIST	3.249074	0.000055	5.206535	0.000101	
	Present study	3.249987	0.000003	5.206790	0.000009	6.82
TiO_2	NIST	4.593939	0.000062	2.958862	0.000063	
	Present study	4.593870	0.000007	2.958872	0.000008	3.91
Cr_2O_3	NIST	4.959610	0.000079	13.597470	0.000250	
	Present study	4.959610	0.000006	13.598314	0.000025	5.35
Si	NIST	5.4311946	0.0000092			
	Present study	5.4311470	0.0000050			8.27

The energy of incident X-radiation can determine important parameters such as the S/N ratio of the recorded XRD patterns, as well as the instrumental resolution. The amplitude of the IP signal for each incident X-ray photon depends on the energy of the X-ray photons and can influence the S/N ratio in the observed XRD pattern. It is considered to be proportional to the product of the absorption efficiency and the amount of energy deposited in the phosphor by an absorbed X-ray photon (Amemiya, 1995). The X-ray absorption of the commercial IPs of type ST III and ST V (Fuji), which are similar to the IP used in the CIP detector, is 100% for energies below 20 keV and decreases to about 50% for energies up to 37 keV (Thoms *et al.*, 1998). Therefore, the effect of incident radiation energy on the S/N ratios of the observed patterns was expected to be minimal for the range of energy over which the CIP detector performance was evaluated in this study. However, absorption of X-rays by the sample is also an important consideration, and is higher for lower-energy photons. The duration of exposure for lower-energy photons was increased in order to achieve S/N ratios similar to the XRD patterns collected using higher-energy photons.

Since the absorption efficiency of the IP is almost 100% in the evaluated energy range, all the photostimulable centers created as a result of the X-ray absorption are expected to be confined to a thin surface layer on the IP. The path of the laser beam used to read the stored information from the site of the X-ray irradiation to the photostimulable centers is very short. This also minimizes broadening of the stimulated intensity profile owing to any bleaching effect. As a consequence, the emitted light which is measured by the PMT represents the X-ray information of a narrower area of the IP, resulting in a higher resolution (Thoms *et al.*, 1998). This is consistent with the observation that the instrumental resolution was not influenced by the incident X-ray photon energy for the energy range studied (14.0 keV to 22.5 keV).

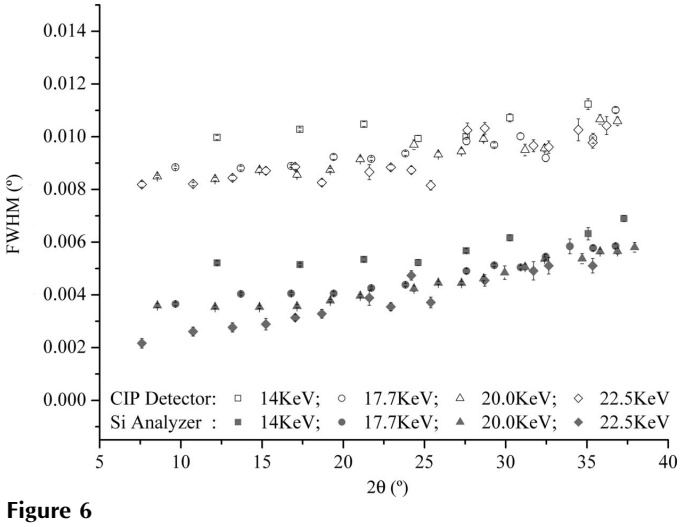

Figure 6
The CIP detector can be operated over a wide range of incident energy with comparable resolution. Data from an analyzer are presented for comparison.

4.4. Crystal structure refinement

Angular resolution and integrated intensities are two very important parameters for structure determination from powder diffraction patterns. Standard powder samples of Si (SRM 640c), α-Al_2O_3, TiO_2, ZnO and Cr_2O_3 (SRM 676a) were used to evaluate the suitability of the CIP detector data for crystal structure refinement. Sample powders were mounted in 0.2 mm glass capillaries and rotated at 60 r.p.m., while XRD patterns were acquired in transmission geometry using X-rays of wavelength 0.5631 Å. The S/N ratio was optimized without saturating the detector by using attenuation filters, by optimizing exposure time and by averaging multiple exposures. The *GSAS* software package (Larson & von Dreele, 1997) was used to model the observed XRD patterns by the Rietveld method (Rietveld, 1969). The starting crystal structure for refinement of each phase was based on ICDD (International Center for Diffraction Data, Newtown Square, PA, USA) or ICSD [International Crystal Structure Database, NIST and Fachinformationszentrum Karlsruhe (FIZ), Germany] files. In the case of Si, ICDD JCPDS no. 04-007-8736 was used; and ICSD nos. 88028, 36412, 94002 and 75577 were used for α-Al_2O_3, TiO_2, ZnO and Cr_2O_3, respectively. Table 3 compares the experimentally refined lattice constants for each standard phase with the NIST-accepted values, and the residual factors from the Rietveld fitting are also included. There is good agreement in the lattice constant values for all the standard samples.

Fig. 7 shows the Rietveld refinement results on the SRM 640c standard. The quality of fit is excellent when the

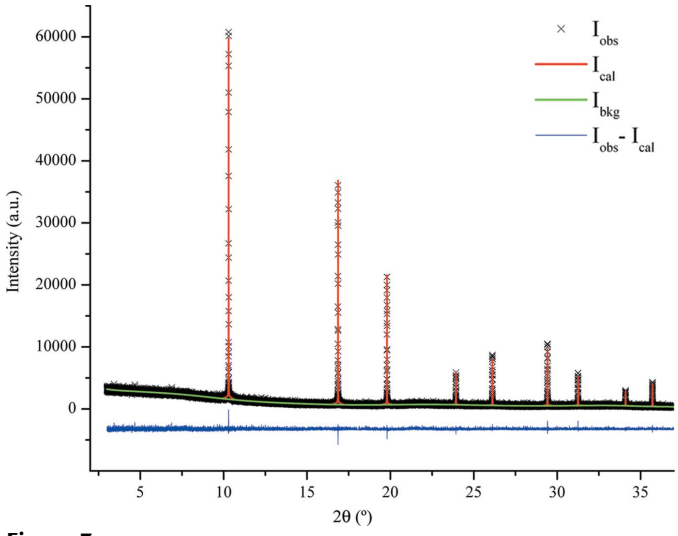

Figure 7
Rietveld refinement of the Si (SRM 640c) powder standard.

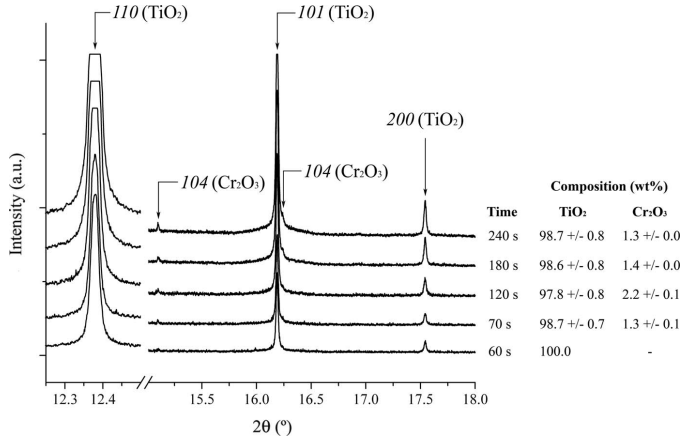

Figure 8
Quantitative determination of the minor phase present in a multiphase mixture by incremental saturation of the high-intensity peaks.

experimental and simulated patterns are compared, as demonstrated in the difference pattern included in the figure. However, the residuals for the fitted profile, which quantifies the goodness of fit, were somewhat larger than desired. The data could only be refined to obtain R_p values of 8.27 (and R_{wp} of 11.01). Besides possible errors in precise positioning of the capillary, it is believed that the inability to accurately model the background was responsible for the higher residual values. The Si sample, unlike other standard samples used in this study, was exposed for only 15 s and the diffraction data were averaged over only six separate exposures to obtain the data set used for Rietveld refinement (note that XRD data from up to ten exposures were averaged for other standard samples).

4.5. Detection of minor phases

The linearity in response of the CIP detector to incident photon flux had highlighted the independence of the detector response for different regions on the CIP detector. This aspect was further explored as a tool for quantitative determination of minor/trace phase content in a multiphase mixture. For this purpose a mixture of two standard powders was prepared and comprised of 1 wt% Cr_2O_3 + 99 wt% TiO_2. Both the powders are standard reference materials (SRM 674a) and their choice was primarily influenced by their similar scattering properties. The powder mixture was mounted in a 0.2 mm capillary and XRD patterns were collected for increasing amounts of exposure time using X-rays of wavelength 0.7006 Å (~17.7 keV). Small segments of the acquired XRD patterns are presented in Fig. 8 for exposure times ranging from 60 s to 240 s. As exposure time was increased, the higher-intensity peaks of the major phase (TiO_2) were saturated, and showed a plateau feature. However, the minor phase peaks, which were immersed in the background for the 60 s exposure, increasingly became apparent at larger exposure times. The phase content was also quantitatively analyzed by whole pattern refinement routines using *JADE* software (MDI, Livermore, CA, USA). The saturated portion of the XRD spectrum was masked during this analysis. The results are included in the inset in Fig. 8, and demonstrate the improved accuracy in quantitative analysis of minor phase content with increasing exposure times.

Despite the saturation of certain diffraction peaks in the XRD pattern collected with the CIP detector, the position and the shapes of the unsaturated peaks were not affected and intensity displayed a linear response to incident photon flux. This characteristic of an IP detector is in contrast with gas-filled PSDs, which are not only limited in their count rate but also in the linearity in response between different angular channels and angular position (Masson *et al.*, 2005). The lack of angular linearity in the gas-filled proportional counter type of PSDs comes from the electronics and the structure of the delay line of the detector (Ballon *et al.*, 1983). The ability to saturate high-intensity peaks to extract minor phase information is a very useful characteristic of the CIP detector, and can benefit various materials science investigations.

4.6. High-temperature X-ray diffraction

The CIP detector has been developed for time-efficient XRD measurements with high resolution which are suitable for structural refinement. The CIP detector was primarily designed for, and has been used with, the QLF in order to conduct rapid HTXRD experiments to study thermal expansions, phase transformations, phase diagrams and kinetics of high-temperature processes (Brennecka *et al.*, 2007; Sarin, Haggerty *et al.*, 2006, 2008; Yoon *et al.*, 2008). The use of QLF for HTXRD investigations on ceramic materials up to 2273 K in air has already been successfully demonstrated (Sarin, Jurkschat *et al.*, 2006; Siah *et al.*, 2005).

In this article the use of the combined CIP + QLF configuration to study the crystallization kinetics of Cs-based geopolymer powders is presented as an example of the HTXRD investigations. Geopolymers are a new class of aluminosilicate materials and are best understood as X-ray amorphous, inorganic, rigid, hydrated gels, which are charge-balanced by group I cations such as Na^{1+}, K^{1+} or Cs^{1+} (Bell *et al.*, 2008). Upon heating, the Cs-based geopolymeric phase

transforms into crystalline pollucite, which is a refractory material (T_{melt} > 2173 K) displaying low thermal expansion characteristics and phase stability up to 1773 K (Bell *et al.*, 2008). HTXRD patterns were collected using powder samples of Cs-based geopolymer mounted in a 0.2 mm quartz capillary (Glas, W. Muller, Schönwalde, Germany) and were normalized for incident photon flux. The powder specimen had 4 wt% Pt powder mixed in it to serve both as an internal standard and as an internal thermometer. Prior treatment had involved heating of the powder mixture to ~973 K to expel any water and to grow the crystallite size of the Pt phase. All the experiments were conducted using 22.5 keV (λ = 0.5508 Å) incident X-radiation in Debye–Scherrer geometry. Since the QLF is capable of heating samples at very fast rates, the desired temperature could be reached within 2 min, and successive HTXRD patterns were acquired under isothermal conditions for more than 30 min. Individual diffraction patterns could be acquired with a time resolution of approximately 120 s. Experiments were repeated at six different temperatures for different durations to determine the extent of crystallization starting from the amorphous geopolymer phase. The XRD patterns were normalized for incident photon flux and were analyzed by whole pattern fitting techniques (Rietveld, 1969) using the *JADE* software.

An example of this isothermal kinetic study conducted at 1398 ± 5 K is shown as a series of HTXRD patterns in Fig. 9. Only a small 2θ range is included to show the changes that occurred as the sample was crystallized. The 0 s scan was collected at 1177 K while the 17 s scan was collected at 1390 K. Quantitative analysis conducted at 1398 ± 5 K confirmed the progress of crystallization and approximately 69% conversion to crystalline pollucite phase was observed in 1853 s. Using this approach, parameters such as activation energy for the crystallization process can be determined. The use of high-speed high-resolution detectors that are capable of simultaneous acquisition of XRD data over a wide angular range is critical for success in dynamic studies (Parise *et al.*, 2000).

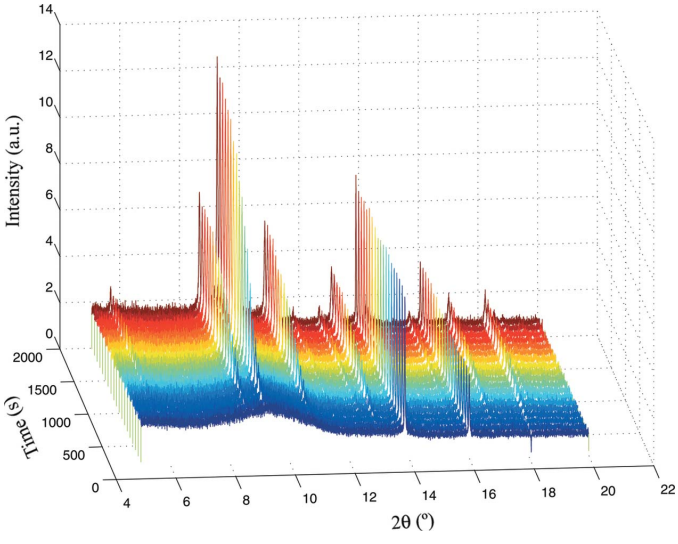

Figure 9
Crystallization of amorphous Cs-geopolymer to pollucite, observed *in situ* at 1398 ± 5 K. Evolution of crystalline phase content was observed with a time resolution of ~2 min. Only a subset of the HTXRD patterns acquired is shown.

5. Summary

A new one-dimensional curved image plate detector has been developed for powder X-ray diffraction investigations using synchrotron radiation. The CIP detector is equipped with an integral reader which enables extraction of X-ray intensity information in ≤30 s. Simultaneous acquisition of diffraction data over a 38.7° 2θ range further augments the suitability of the CIP detector for kinetic studies, as there is no time dependence in the diffraction pattern acquired from a single exposure. The design of the CIP detector also allows the use of a crystal analyzer detector to acquire highest-resolution XRD data without any change in the experimental set-up. The CIP detector is capable of rapid high-resolution X-ray diffraction studies suitable for structural refinement. A variety of experiments were conducted to validate the performance and the capabilities of the CIP detector. The CIP detector is capable of detecting and quantifying minor/trace phases present in a multiphase sample. The high-intensity Bragg peaks of the major phase can be saturated to make minor phase peaks more apparent, without compromising the linearity and uniformity in the detector response. Together with a thermal image furnace which can be used to heat samples up to 2273 K in air, high-resolution HTXRD studies are now possible in real time. It is anticipated that the variety of investigations that are now possible using the CIP detector will considerably broaden the fields of materials research accessible through X-ray diffraction, and will also accelerate the development of materials to address the emerging challenges.

The CIP detector was designed and built under an AFOSR DURIP grant, number FA9550-04-1-0345. The authors were supported under the following grants for the duration of this work: AFOSR grant FA9550-06-1-0386 for PS and RPH; AFOSR grant F49620-03-1-0082 for WY; NSF grant NSF DMR 02-11139 for PS for one year. Use of the Advanced Photon Source at Argonne National Laboratory was supported by the US Department of Energy, Office of Science, Office of Basic Energy Sciences, under contract No. DE-AC02-06CH11357.

References

Amemiya, Y. (1995). *J. Synchrotron Rad.* **2**, 13–21.
Amemiya, Y. & Miyahara, J. (1988). *Nature (London)*, **336**, 89–90.
Arndt, U. W. (1986). *J. Appl. Cryst.* **19**, 145–163.
Ballon, J., Comparat, V. & Pouxe, J. (1983). *Nucl. Instrum. Methods Phys. Res.* **217**, 213–216.
Bell, J. L., Sarin, P., Provis, J. L., Haggerty, R. P., Driemeyer, P. E., Chupas, P. J., van Deventer, J. S. J. & Kriven, W. M. (2008). *Chem. Mater.* **20**, 4768–4776.
Brennecka, G. L., Payne, D. A., Sarin, P., Zuo, J. M., Kriven, W. M. & Hellwig, H. (2007). *J. Am. Ceram. Soc.* **90**, 2947–2953.

Caglioti, G., Paoletti, A. & Ricci, F. P. (1958). *Nucl. Instrum.* **3**, 223–228.
Evain, M., Deniard, P., Jouanneaux, A. & Brec, R. (1993). *J. Appl. Cryst.* **26**, 563–569.
Fauth, F., Bronnimann, C., Auderset, H., Maehlum, G., Pattison, P. & Patterson, B. (2000). *Nucl. Instrum. Methods Phys. Res. A*, **439**, 138–146.
Fitch, A. N. (2004). *J. Res. Nat. Inst. Standards Technol.* **109**, 133–142.
Fujiwara, A. *et al.* (2000). *J. Appl. Cryst.* **33**, 1241–1245.
Garrett, R. F., Cookson, D. J., Foran, G. J., Sabine, T. M., Kennedy, B. J. & Wilkins, S. W. (1995). *Rev. Sci. Instrum.* **66**, 1351–1353.
Gualtieri, A., Norby, P., Hanson, J. & Hriljac, J. (1996). *J. Appl. Cryst.* **29**, 707–713.
Hall, C. & Lewis, R. (1994). *Nucl. Instrum. Methods Phys. Res. A*, **348**, 627–630.
Hastings, J. B., Thomlinson, W. & Cox, D. E. (1984). *J. Appl. Cryst.* **17**, 85–95.
Kellermann, G., Neuenschwander, R., Feugeas, J. & Craievich, A. F. (2001). *Nucl. Instrum. Methods Phys. Res. A*, **467**, 1097–1100.
Knapp, M., Baehtz, C., Ehrenberg, H. & Fuess, H. (2004). *J. Synchrotron Rad.* **11**, 328–334.
Knapp, M., Joco, V., Baehtz, C., Brecht, H. H., Berghaeuser, A., Ehrenberg, H., von Seggern, H. & Fuess, H. (2004). *Nucl. Instrum. Methods Phys. Res. A*, **521**, 565–570.
Larson, A. C. & von Dreele, R. B. (1997). *GSAS – General Structure Analysis System.* Document LAUR 86-748. Los Alamos National Laboratory, New Mexico, USA.
Lee, P. L., Shu, D., Ramanathan, M., Preissner, C., Wang, J., Beno, M. A., Von Dreele, R. B., Ribaud, L., Kurtz, C., Antao, S. M., Jiao, X. & Toby, B. H. (2008). *J. Synchrotron Rad.* **15**, 427–432.
Masson, O., Boulle, A., Guinebretire, R., Lecomte, A. & Dauger, A. (2005). *Rev. Sci. Instrum.* **76**, 063912.
Miyahara, J., Takahashi, K., Amemiya, Y., Kamiya, N. & Satow, Y. (1986). *Nucl. Instrum. Methods Phys. Res. A*, **246**, 572–578.
Nishibori, E., Takata, M., Kato, K., Sakata, M., Kubota, Y., Aoyagi, S., Kuroiwa, Y., Yamakata, M. & Ikeda, N. (2001*a*). *J. Phys. Chem. Solids*, **62**, 2095–2098.
Nishibori, E., Takata, M., Kato, K., Sakata, M., Kubota, Y., Aoyagi, S., Kuroiwa, Y., Yamakata, M. & Ikeda, N. (2001*b*). *Nucl. Instrum. Methods Phys. Res. A*, **467**, 1045–1048.
Norby, P. (1997). *J. Appl. Cryst.* **30**, 21–30.
Parise, J. B., Cahill, C. L. & Lee, Y. (2000). *Can. Mineral.* **38**, 777–800.
Rietveld, H. M. (1969). *J. Appl. Cryst.* **2**, 65–71.
Rizzo, F., Doyle, S. & Wroblewski, T. (1995). *Nucl. Instrum. Methods Phys. Res. B*, **97**, 479–482.
Sarin, P., Haggerty, R. P., Yoon, W., Kriven, W. M., Knapp, M. & Zschack, P. (2006). *Ceram. Eng. Sci. Proc.* **27**, 313–324.
Sarin, P., Yoon, W., Haggerty, R. P., Chiritescu, C., Bhorkar, N. C. & Kriven, W. M. (2008). *J. Eur. Ceram. Soc.* **28**, 353–365.
Sarin, P. Y. W., Jurkschat, K., Zschack, P. & Kriven, W. M. (2006). *Rev. Sci. Instrum.* **77**, 093906.
Seggern, H. von (1999). *Braz. J. Phys.* **29**, 254–268.
Shishiguchi, S., Minato, I. & Hashizume, H. (1986). *J. Appl. Cryst.* **19**, 420–426.
Siah, L. F., Kriven, W. M. & Schneider, J. (2005). *Meas. Sci. Technol.* **16**, 1–8.
Siddons, D. P., Hulbert, S. L. & Stephens, P. W. (2007). *AIP Conf. Proc.* **879**, 1767–1770.
Sonoda, M., Takano, M., Miyahara, J. & Kato, H. (1983). *Radiology*, **148**, 833–838.
Ståhl, K. (2000). *J. Appl. Cryst.* **33**, 394–396.
Thoms, M., Bauchau, S., Häusermann, D., Kunz, M., Bihan, T. L., Mezouar, M. & Strawbridge, D. (1998). *Nucl. Instrum. Methods Phys. Res. A*, **413**, 175–184.
Thoms, M., Burzlaff, H., Kinne, A., Lange, J., von Seggern, H., Spengler, R. & Winnacker, A. (1996). *Mater. Sci. Forum*, **228–231**, 107–112.
Toby, B. H. (2005). Toby, B. H. (2005). *CMPR.* Version 1.34. *Crystallography Software: Download Links at the NIST Center for Neutron Research*, http://www.ncnr.nist.gov/xtal/software/downloads.html.
Wölfel, E. R. (1983). *J. Appl. Cryst.* **16**, 341–348.
Yoon, W., Sarin, P. & Kriven, W. M. (2008). *J. Eur. Ceram. Soc.* **28**, 455–463.